

Broadband and Omnidirectional Anti-reflection Layer for III/V Multi-junction Solar Cells

Silke L. Diedenhofen^{a,1,*}, Grzegorz Grzela^a, Erik Haverkamp^b, Gerard Bauhuis^b, John Schermer^b, Jaime Gómez Rivas^{a,d,**}

^a*FOM Institute AMOLF, c/o Philips Research Laboratories, High-Tech Campus 4, 5656 AE Eindhoven, The Netherlands*

^b*Radboud University Nijmegen, Institute for Molecules and Materials, Applied Materials Science, Heyendaalseweg 135, 6525 AJ Nijmegen, The Netherlands*

^c*Philips Research Laboratories, High-Tech Campus 4, 5656 AE Eindhoven, The Netherlands*

^d*COBRA Research Institute, Eindhoven University of Technology, P.O. Box 513, 5600 MB Eindhoven, The Netherlands*

Abstract

We report a novel graded refractive index antireflection coating for III/V quadruple solar cells based on bottom-up grown tapered GaP nanowires. We have calculated the photocurrent density of an InGaP-GaAs-InGaAsP-InGaAs solar cell with a MgF₂/ZnS double layer antireflection coating and with a graded refractive index coating. The photocurrent density can be increased by 5.9 % when the solar cell is coated with a graded refractive index layer with a thickness of 1 μm. We propose to realize such a graded refractive index layer by growing tapered GaP nanowires on III/V solar cells. For a first demonstration of the feasibility of the growth of tapered nanowires

*Corresponding author

**Principal corresponding author

Email addresses: `diedenhofen@amolf.nl` (Silke L. Diedenhofen), `rivas@amolf.nl` (Jaime Gómez Rivas)

¹Present address: ICFO - The Institute of Photonic Sciences, Av. Carl Friedrich Gauss, 3, 08860 Castelldefels (Barcelona), Spain.

on III/V solar cells, we have grown tapered GaP nanowires on AlInP/GaAs substrates. We show experimentally that the reflection from the nanowire coated substrate is reduced and that the transmission into the substrate is increased for a broad spectral and angular range.

Keywords:

III/V Solar cells, anti-reflection, semiconductor nanowires

1. Introduction

Over the last years the photovoltaic research has brought many solutions to increase the efficiency of solar cells. While triple junction solar cells with efficiencies exceeding 40 % have been demonstrated [1, 2], research is focusing now on the realization of quadruple solar cells [3]. These solar cells have expected efficiencies exceeding 50 % [4]. However, for this type of solar cells, the standard double layer antireflection coatings are not sufficient for reducing the reflection over the broad wavelength range that is absorbed by the multiple junctions [3, 5]. The standard double layer antireflection coatings typically have a bandwidth lower than one octave, e.g., 400 nm to 700 nm or 800 nm to 1100 nm [6], while quadruple solar cells require an antireflection coating operating from ~ 350 nm to ~ 1700 nm [4]. To approach an optimal performance and the maximum efficiency that has been theoretically calculated broad-band antireflection layers are necessary. The spectral range of an antireflection coating is not the only factor limiting the efficiency of multi-junction solar cells. As these solar cells will be mainly installed in solar concentrator systems, the angular response has to be optimized as well.

One way to achieve the desired broadband and omni-directional antire-

flection layers is by employing the so-called moth-eye concept [7]. In this concept, nanostructures forming an effective medium result in a gradual increase of the refractive index from that of air ($n = 1$) to that of the solar cell medium ($n \sim 3.3$). Recently, different graded refractive index layers have been demonstrated [8–16]. These subwavelength structures can be achieved in different ways, e.g., by etching nanostructures into the surface [9, 12–16], or by oblique-angle deposition [8], or by chemical deposition of nanostructures [10, 11]. When the nanostructures are fabricated by etching, the material of the nanostructures is typically the same forming the active layer of the solar cell. Deposition of nanostructures offers a wider range of materials for the nanostructures, thus higher flexibility in the design of antireflection coatings[8, 10, 11].

It has been recently demonstrated that graded refractive index layers can be fabricated by bottom-up grown tapered GaP nanowires or layers of nanowires with a broad distribution of nanowire lengths [11]. The nanowires were grown on a GaP substrate, and an increased transmission through the GaP substrate with respect to a bare GaP substrate was demonstrated. The bottom-up growth method used for fabricating nanowires allows hetero-epitaxial growth of a passive antireflection layer on top of the active layer of the solar cell. Having a passive antireflection layer is advantageous because of the following reasons: Surface carrier recombination can be dominant in active nanostructured materials due to their large surface. This effect is not relevant in the case of passive nanostructures, such as the proposed antireflection nanowire layers, since light is not absorbed in these structures. Carriers are only generated in the active multi-junction solar cell, beneath

the nanowire coating, where they can be separated and extracted.

In this manuscript, we calculate the photocurrent densities of III/V quadruple solar cells covered with different antireflection coatings. These calculations reveal that a graded refractive index layer increases the photocurrent density of the solar cell with respect to a solar cell coated with a standard MgF_2/ZnS double layer antireflection coating. We propose to realize such graded refractive index layers with tapered GaP nanowires and demonstrate the growth of tapered GaP nanowires on a layer of AlInP that is lattice matched to GaAs. We use GaP nanowires because of the large refractive index of GaP ($n \simeq 3.3$) and its high electronic bandgap energy ($\lambda_{\text{gap}} = 549 \text{ nm}$). AlInP is used as substrate for the nanowire growth because it is considered the most suitable material to form the upper window layer in a quadruple III/V solar cell structure [12]. Furthermore, we have measured the reflectance and transmittance of an AlInP/GaAs substrate coated with nanowires and without nanowires. We find that the layer of tapered nanowires reduces the total reflectance from the AlInP/GaAs substrate for a broad range of wavelengths and concomitantly increases the omni-directional transmission into and absorption in the AlInP/GaAs substrate. These measurements constitute a proof-of-principle as they are the first experimental verification that tapered GaP nanowires could be used as an antireflection layer for III/V solar cells.

2. Anti-reflection Layers

To show that the efficiency of a III/V quadruple solar cell can be increased by adding a graded refractive index layer, we have calculated the

reflection from and transmission through an AlInP window layer coated with different anti-reflection layers. For these calculations the III/V solar cell was considered to consist of InGaP, GaAs, InGaAsP, and InGaAs with electronic bandgaps that correspond to cut-off wavelengths of respectively 649 nm, 873 nm, 1215 nm, and 1770 nm. The calculations are performed using the transfer-matrix method [17]. The refractive index of AlInP varies from 3.06 - 2.14i at 350 nm to 2.77 at 1700 nm, and the refractive index of GaAs from 3.28 - 2.06i at 350 nm to $3.36 - 5.32 \cdot 10^{-5}i$ at 1700 nm. These values have been determined from ellipsometry measurements of the materials used in the experiments shown in the next section. The refractive indices of ZnS and MgF₂ vary between 2.8 - 0.13i and 2.27, and 1.38 and 1.37, respectively for wavelengths between 350 nm and 1700 nm. Figure 1 shows the calculated reflectance from an AlInP layer with a thickness of 30 nm coated with different anti-reflection layers in (a) linear and (b) logarithmic scale. The black solid curves in Figures 1a and b show the calculated reflectance of the bare AlInP layer without antireflection coating. The reflectance from an AlInP layer coated with a MgF₂/ZnS double layer antireflection coating with thicknesses of 89 nm (ZnS) and 105 nm (MgF₂) is displayed by the red long-dashed curves in Figures 1a and b. The calculated reflectance from that coating is lower than 10 % for wavelengths between 450 nm and 1730 nm. While this anti-reflection coating reduces the reflection for a rather broad wavelength range, the bandwidth is not optimal for reducing the reflectance over the wavelength range in which III/V multi-junction solar cells absorb light.

To show that the bandwidth of low reflectance can be increased by a graded refractive index layer, we have calculated the reflectance from a 30 nm

thin AlInP layer that is coated with three different lossless graded refractive index layers. A schematic of the layout used in the calculations is given in the inset of Figure 1a, in which a change in color represents a change in refractive index. The refractive index of these layers is parabolically increasing from 1.0 to 3.3, and the thicknesses of the layers are 250 nm, 500 nm, and 1000 nm, respectively. In the transfer-matrix calculation, the anti-reflection layer is implemented by considering sublayers with a thickness of 10 nm and the refractive index is increased parabolically from one layer to the next. These calculations are displayed in Figures 1a and b by the olive-short-dashed, the blue dash-dotted, and the magenta dashed-dot-dotted curves, respectively. While the graded refractive index layer with a thickness of 250 nm does not decrease the reflectance significantly for wavelengths longer than 850 nm, the reflectance of the graded refractive index layers with a thickness of 500 nm and 1000 nm are around 1 % or lower for a broad wavelength range. The reflection is the lowest, when a 1000 nm thick graded refractive index antireflection coating is applied to the multi-junction solar cell. In this coating, the gradient of the refractive index between adjacent sublayers is the smallest.

Corresponding to the reflectance calculations, we have performed calculations of the transmittance through a 30 nm thin AlInP layer coated with the same anti-reflection layers as above. The calculated transmittance is shown in Figures 1c and d in linear and logarithmic scale, respectively. From the calculated transmittance, we have determined the solar spectrum weighted transmittance $SSWT$ of the different layers by

$$SSWT = \frac{\int F(\lambda) \cdot T(\lambda) d\lambda}{\int F(\lambda) d\lambda}, \quad (1)$$

where $F(\lambda)$ and $T(\lambda)$ are the photon flux (AM1.5G, 1000 W/m²) and the calculated transmittance, respectively. The integration is performed in the wavelength range from 300 nm to 1760 nm. The solar weighted transmittances of the 5 different samples are 69.2 % for a bare solar cell, 86.3 % for the MgF₂/ZnS antireflection coating, 89 % for the 250 nm thick graded refractive index layer, 91.5 % for the 500 nm thick graded refractive index layer, and 91.7 % for the 1 μ m thick graded refractive index layer. Therefore, the solar weighted transmittance can be increased by 6.3 % when the 1 μ m thick graded refractive index layer is used as an antireflection layer instead of the double layer MgF₂/ZnS coating.

According to the calculations of reflectance from and transmittance through the AlInP layer, we have determined the reflectance from and transmittance through each individual layer of a III/V multi-junction solar cell. We have modeled the optical multilayer structure using the transfer-matrix method [18]. With this method, we have calculated the reflectance and transmittance at each interface. From these transmittances and reflectances, we have determined the absorption in each sublayer. Multiplying the absorption in each subcell by the photon flux results in the amount of photons absorbed in each subcell. The internal quantum efficiency (IQE) of each sub cell is set to unity, meaning that every photon absorbed in one of the layers contributes to the photocurrent density of the cell. With this IQE the electron-hole pair generation is calculated, resulting in a sub-cell specific photocurrent. This method allows to calculate an unlimited amount of optical layers but it is limited by the difficulties in predicting the reflections between sub-cells. The model has been verified by comparing the calculated reflection of a single

junction solar cell coated with different antireflection layers to the measured reflection [18]. The photocurrent densities in each subcell and the resulting photocurrent density of the quadruple solar cell are given in Table 1 for a solar cell coated with a perfect antireflection coating, without antireflection coating, with a MgF_2/ZnS double-layer antireflection coating, and with graded refractive index layers with parabolically increasing refractive index from 1.0 to 3.3 over a thickness of 250 nm, 500 nm, and 1000 nm. The first column in Table 1 shows the maximum photocurrent densities and the maximum efficiency of the solar cell if a perfect anti-reflection layer is used, i.e., all incident light within the absorption band of the solar cell is transmitted into and absorbed in the solar cell. The maximum photocurrent density that can be achieved when all incident light is absorbed is 13.36 mA/cm^2 . When applying a graded refractive index layer with a thickness of 1000 nm and a parabolically increasing refractive index from 1 to 3.3 to the solar cell, a photocurrent density of 13.28 mA/cm^2 can be achieved. This photocurrent density is limited by the bottom cell. The calculated photocurrent density in the solar cell coated with the MgF_2/ZnS double layer antireflection coating is 12.54 mA/cm^2 and is in all subcells lower than the photocurrent density in the solar cell coated with the thickest graded refractive index layer. The photocurrent density in the solar cell coated with this graded refractive index layer is increased by 5.9 % with respect to that of the cell with the double layer antireflection coating.

3. Tapered GaP Nanowires

To investigate the feasibility of nanowire graded refractive index layers on top of multijunction solar cells, we have grown layers of tapered GaP nanowires on top of AlInP using the vapor-liquid-solid (VLS) growth mechanism [19] by metal-organic vapor phase epitaxy (MOVPE). AlInP is commonly used as upper window layer in III/V solar cells [12]. For matching the growth conditions to that of a real solar cell device, we have grown 30 nm of AlInP on top of a polished (100) n^{++} -doped GaAs wafer. This AlInP layer has been protected by a 300 nm thick GaAs layer. Before nanowire growth, we have removed this GaAs layer by etching the substrate in 28% $\text{NH}_4\text{OH} : \text{H}_2\text{O}_2 : \text{H}_2\text{O}$ (1 : 1 : 100). Immediately after this etching step, gold with an equivalent layer thickness of 0.3 nm has been evaporated and the gold coated substrate has been placed in the MOVPE reactor. The GaP nanowires are grown for 180 seconds at a temperature of 570 °C using trimethyl-gallium (TMG) and phosphine (PH_3) as precursors. A top-view scanning electron micrograph of the GaP nanowires grown on AlInP is shown in Figure 2a. The nanowires are grown epitaxially with preferential growth in the $\langle 111 \rangle$ direction, however, some nanowires also grow normal to the substrate. From the cross-sectional scanning electron micrograph in Figure 2b, the thickness of the nanowire layer can be determined to be 600 ± 100 nm. The variation of the layer thickness can be attributed to nanowires growing into different crystallographic directions with different growth rates.

To determine the effect of the tapered nanowires on the reflection and transmission, we have measured the total reflectance and the diffuse reflectance from the AlInP/GaAs substrate and the AlInP/GaAs substrate

coated with tapered nanowires. We have measured the total reflectance from both samples using a Lambda 950 spectrometer (PerkinElmer) consisting of a tungsten-halogen and a deuterium lamp, an integrating sphere, and a photomultiplier tube. For the reflectance measurements, the samples have been mounted at the backside of the integrating sphere. The angle of incidence was 8° , allowing the measurement of the total and diffusely reflected light. The diffusely reflected light is measured by making a small opening in the integrating sphere in such a way that the specularly reflected light escapes from the sphere. The reflection measurements on the samples are normalized by the reflection of a white-standard to obtain the absolute reflectance of the array. From the total reflectance, R , and the diffuse reflectance, R_{dif} , the specular reflectance, R_{spec} , can be determined by $R_{\text{spec}} = R - R_{\text{dif}}$. Figure 3a displays the measured total reflectance (black squares), diffuse reflectance (red circles), and the resulting specular reflectance (blue triangles) from the AlInP/GaAs substrate. The total and specular reflectance is similar (28 %) at wavelengths below the electronic bandgap of GaAs (865 nm), and the diffuse reflectance is negligible. This low diffuse reflectance is expected for a flat layer. For wavelengths longer than 865 nm, the reflectance increases to 36 %, as the reflectance of the backside of the substrate is contributing to the measurement. At these wavelengths, the diffuse reflectance is slightly increased, indicating that the backside of the sample is rougher than the front side. From these two measurements, we can understand the contribution to the reflection of the substrate backside and the AlInP front side of the sample. The black solid curve in Figure 3a shows a calculation of the specular reflection of an AlInP/GaAs layer for comparison done with the transfer matrix

method. For this calculation, we have slightly varied the refractive indices of AlInP and GaAs for fitting the measurements. The resulting refractive index of AlInP varies from $n = 3.82 - 0.24i$ at 400 nm to 3.04 at 2000 nm, the refractive index of GaAs varies from $n = 3.86 - 2.27i$ at 400 nm to $3.15 - 10^{-4}i$ at 2000 nm. These refractive indices are the only fitting parameters in the determination of the reflection.

In a next step, we have measured the total and diffuse reflectance from the AlInP/GaAs substrate coated with tapered nanowires. These measurements are displayed in Figure 3b. The total reflectance (black squares) is strongly reduced compared to the measurement of the AlInP/GaAs substrate. While the total reflectance is lower than 10 % at wavelengths below 873 nm, the total reflectance increases for wavelengths above the electronic bandgap of GaAs as in the case of the bare AlInP/GaAs substrate. This increased total reflectance can be attributed to the reflectance of the back-side of the substrate. The diffuse reflectance (red circles) is dominating the total reflectance for wavelengths shorter than 873 nm. The increasing diffuse reflectance with decreasing wavelength is expected and due to scattering of light from the thick bottom part of the nanowires [20]. For wavelengths longer than 865 nm, the diffuse reflectance is similar to that of the AlInP/GaAs substrate, indicating that scattering of light from the nanowires is negligible at these wavelengths.

Although these first measurements demonstrate that the reflectance of the AlInP/GaAs substrate coated with tapered nanowires is significantly reduced with respect to the bare AlInP/GaAs substrate, the reflectance of the nanowire sample needs to be further decreased for a perfect anti-reflection

coating. Therefore, a smaller gradient of the refractive index has to be realized. Further, the bottom diameter of the nanowires has to be decreased to reduce the diffuse reflection at short wavelengths and the density of nanowires has to be increased to achieve a high index of refraction at the interface with the AlInP. The dashed curve in Figure 3b shows a fit to the measurements using the transfer matrix method. The spatial dependence of the refractive index was used as a fitting parameter, obtaining a parabolic increase from 1.1 at the air-nanowire interface to 1.4 at the nanowire-substrate interface. While the fit describes the measurement quantitatively at wavelengths longer than 870 nm, it is limited at visible wavelengths due to the scattering of light by the nanowires. We consider the layer homogeneous for the fit, neglecting this scattering in the calculation. Due to the scattering, the Fabry-Pérot oscillations that are visible in the calculation are not present in the measurements. Further, the fit overestimates the reflectance as light is preferentially scattered into the substrate with a high refractive index [21].

To determine the enhancement of the coupling of light into the AlInP/GaAs substrate by the tapered nanowires, we have measured the total transmittance through the AlInP/GaAs substrate (solid squares in Figure 3c) and through the AlInP/GaAs substrate coated with tapered nanowires (open squares). The solid and dashed curves in Figure 3c show the calculated transmittance through the AlInP/GaAs substrate and the nanowire sample, respectively. For wavelengths below 873 nm, the transmission is negligible in both measurements, as the light gets absorbed in the 360 μm thick GaAs substrate. For wavelengths above the electronic bandgap of GaAs (865 nm), the transmittance through the bare AlInP/GaAs substrate increases strongly,

reaching 43 % for wavelengths longer than 950 nm. The transmittance through the AlInP/GaAs substrate coated with tapered nanowires is 47 %. This transmittance in both measurements is influenced by residual free-carrier absorption for wavelengths above the electronic bandgap of GaAs, which also causes the rather low increase of the transmittance through the AlInP/GaAs substrate coated with nanowires with respect to the bare AlInP/GaAs substrate. This residual absorptance A can be determined by $A = 100\% - R - T$, with R and T being the total reflectance and transmittance, respectively. The absorptance in the AlInP/GaAs substrate and in the AlInP/GaAs substrate coated with tapered nanowires is displayed in Figure 3d. The absorption in the nanowire coated sample (open squares) is increased with respect to the uncoated substrate (solid squares) for all wavelengths. For the wavelength range below 873 nm, the fact that less light is reflected is the main cause for the enhanced absorption (absorptance higher than 90%) in the sample coated with nanowires. For the wavelength range above 873 nm, the increased absorption might be attributed to diffusely transmitted light due to the nanowires. The diffusely transmitted light travels through the GaAs with a longer optical path length, resulting in a higher absorption probability due to free-carrier absorption. The solid and dashed curves in Figure 3d show the calculated absorptance of the AlInP/GaAs substrate and the nanowire sample, respectively, using the transfer matrix method. According to the calculation of the reflectance of the nanowire sample, the calculated absorptance in the nanowire sample is underestimated. The inset in Figure 3d shows a photograph of the AlInP/GaAs substrate coated with nanowires (sample on the left) and without nanowires (sample

on the right). The bare substrate is shiny silverish, as expected from GaAs. The sample coated with nanowires is black, demonstrating the high absorption in the sample.

Analog to the calculations performed for determining the photocurrent of the solar cells displayed in Table 1, we have calculated the photocurrent of a solar cell coated with an antireflection layer that is gradually increased from 1.1 to 1.4 over a thickness of 600 nm, resembling our measurements. A solar cell coated with such an antireflection layer would have a total current of 10.98 mA/cm². This total current is increased by 1.5 mA/cm² compared to a bare cell. However, the calculation only represents a lower limit of the increase in photocurrent, as the absorptance in the solar cell obtained from the calculation is underestimated with respect to the expected absorption from the experiments. We note that while the estimated photocurrent is lower than the photocurrent of a solar cell coated with a double-layer antireflection coating, the graded refractive index layer can be significantly improved by growing a nanowire layer with a higher material filling fraction at the bottom.

Because the tapered nanowires are grown preferentially into the $\langle 111 \rangle_B$ direction, we could expect that the transmittance through the sample is anisotropic, i.e., the transmittance depends on the azimuthal angle of the sample. To determine this anisotropy, we have measured the zero-order transmission through the AlInP/GaAs substrate coated with the tapered nanowires for different azimuthal angles. Figure 4 displays the transmittance measured at 1100 nm as a function of azimuthal angle. The rather constant transmittance with respect to this angle indicates that the preferential growth

along the $\langle 111 \rangle_B$ direction does not give rise to an anisotropic response. The transmittance varies between 43.7 % and 46.6 %. These values are slightly lower than the total transmission, indicating that a small fraction of the intensity is diffusely scattered. Importantly, the specular transmittance is for all azimuthal angles higher than that measured through the bare AlInP/GaAs substrate, which is 38.8 % at 1100 nm.

As multi-junction solar cells are usually installed in concentrator systems, the desired anti-reflection coating should omnidirectionally reduce the reflection and increase the transmission into the solar cell. To determine the omnidirectionality of the response of the antireflection layer, we have measured the angle dependent zero-order transmission through the AlInP/GaAs substrate coated with tapered nanowires and normalized it to the transmission through the AlInP/GaAs substrate for unpolarized light. This measurement is displayed in Figure 5. For all wavelengths and angles up to 60° , the normalized transmission is above unity, meaning that for all wavelengths and angles, the transmission into the AlInP/GaAs layer is increased by the presence of the nanowire layer. The insets in Figure 5 show cuts to the measurement at a wavelength of 1400 nm as a function of angle of incidence, and at an angle of incidence of 30° as a function of wavelength. These cuts show that overall the transmission is enlarged by around 20 % and it further increased to 25 % for angles of incidence larger than 50° . In a Fresnel lens based concentrator system the light is typically incident over angles from 0° to 30° , however, higher angles of incidence would allow thinner concentrator modules.

To determine if the nanowire layer is robust to the high irradiance level in concentrator systems, we have illuminated the sample with 125 suns

(AM1.5G) for 4 hours. During the illumination, the sample was mounted on a Cu base for temperature control and the temperature of the sample was kept at 50 °C. We have measured the reflection before and after illumination on 5 different positions of the sample, and found that there is no significant difference between the measurements. From the reflection measurements before and after illumination with 125 suns, we can conclude that the nanowire layer is stable under concentrated sunlight.

4. Conclusions

In conclusion, we have presented calculations demonstrating that the photocurrent density of a III/V quadruple solar cell can be increased when applying a graded refractive index coating to the solar cell instead of the standard MgF_2/ZnS double layer antireflection coating. For demonstrating the feasibility of graded refractive index layers on solar cells, we have grown layers of tapered GaP nanowires on AlInP/GaAs substrates and we have investigated the transmission and reflection properties of these layers. We have shown that the reflection from AlInP/GaAs substrates can be reduced by coating the substrate with a graded refractive index layer. Our experiments reveal that the total reflection is indeed reduced over a broad spectral range when applying tapered GaP nanowires on top of an AlInP/GaAs substrate and that the transmission into the substrate is increased for a wide spectral and angular range. These results render tapered nanowires a promising candidate for increasing the efficiency of III/V multi-junction solar cells.

Acknowledgement

We thank G. Immink for the growth of the nanowires, E. van Thiel for technical assistance, J. Hoppenbrouwer for SEM analysis, and Peter Thijs and Thierry de Smet for useful discussions. This work is part of the research program of the "Stichting voor Fundamenteel Onderzoek der Materie (FOM)", which is financially supported by the "Nederlandse organisatie voor Wetenschappelijk Onderzoek (NWO)" and is part of an industrial partnership program between Philips and FOM.

Table 1: Calculated photocurrent densities of a III/V quadruple junction solar cell coated with a perfect antireflection layer (AM 1.5G), a bare cell without antireflection layer, a MgF₂/ZnS double layer antireflection coating with thicknesses of 89 nm (ZnS) and 105 nm (MgF₂) (AR layer), and different graded refractive index (GI) anti-reflection layers that have a parabolically increasing refractive index from 1.0 to 3.3 over the given thickness.

| | AM1.5G | Bare | AR | 250 | 500 | 1000 |
|---|--------|-------|-------|-------|-------|-------|
| | cell | | layer | nm | nm | nm |
| | | | | GI | GI | GI |
| | | | | layer | layer | layer |
| Top cell current [mA/cm ²] | 16.71 | 10.83 | 12.54 | 13.81 | 13.8 | 13.82 |
| Second cell current [mA/cm ²] | 15.4 | 11.45 | 14.4 | 14.88 | 15.09 | 15.08 |
| Third cell current [mA/cm ²] | 14.98 | 10.86 | 14.72 | 14.16 | 14.9 | 14.94 |
| Bottom cell current [mA/cm ²] | 13.36 | 9.57 | 12.54 | 11.91 | 13.13 | 13.28 |
| Resulting current [mA/cm ²] | 13.36 | 9.57 | 12.54 | 11.91 | 13.13 | 13.28 |

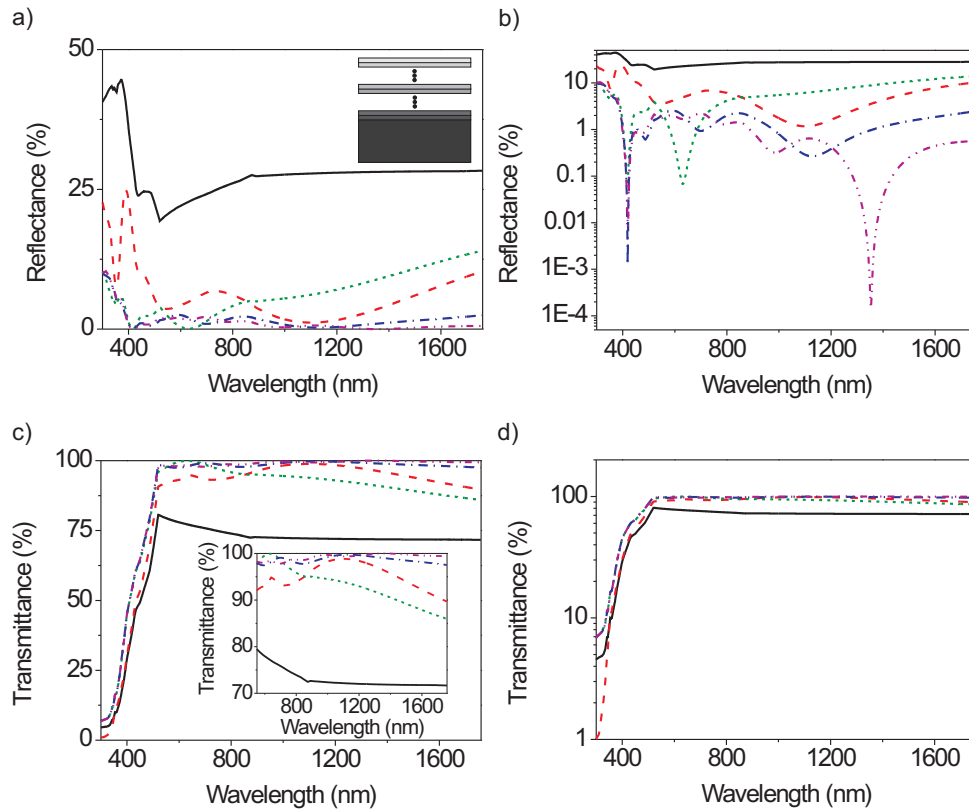


Figure 1: a) and b) Calculation of the reflectance from and c) and d) transmittance through a 30 nm thin AlInP layer coated with different anti-reflection layers in linear scale (a,c) and logarithmic scale (b,d). The black solid curves correspond to the reflectance and transmittance of a bare AlInP layer on top of GaAs substrate. The AlInP layer is coated with a MgF_2/ZnS anti-reflection layer with thicknesses of 89 nm (ZnS) and 105 nm (MgF_2) (red dashed curves), a parabolically increasing refractive index layer from 1.0 to 3.3 with a thickness of 250 nm (olive short-dashed curves), 500 nm (blue dash-dotted curves), and 1 μm (magenta dash-dot-dotted curves). The inset in a) displays a schematic of the layout of the calculations in which a change in color represents a change in refractive index. The inset in c) shows the same calculations as in c) but in a narrower wavelength range.

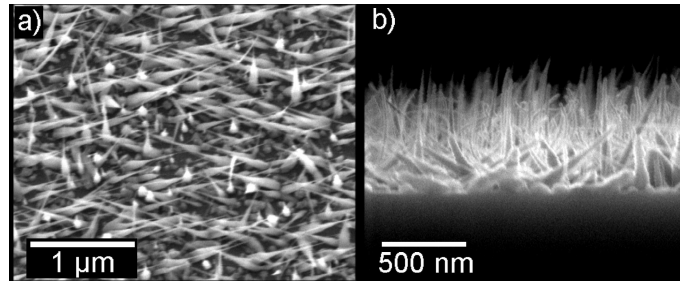


Figure 2: a) Top-view and b) cross-sectional scanning electron micrographs of GaP nanowires grown on AlInP.

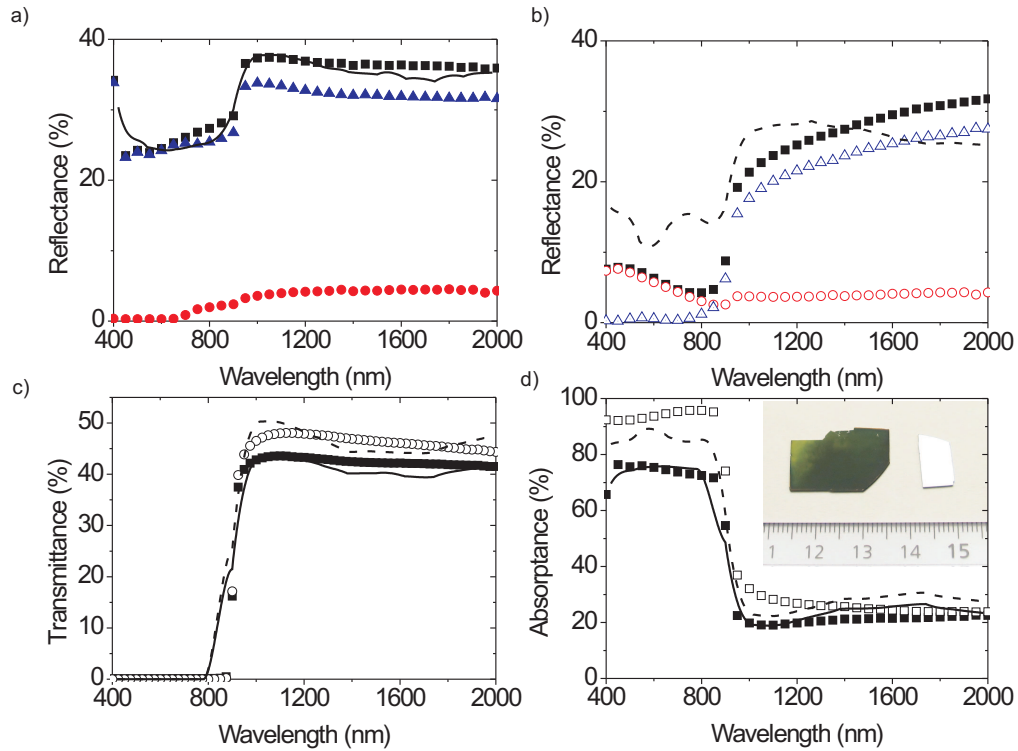


Figure 3: a) Measured reflectance from the AlInP/GaAs substrate and b) measured reflectance from the AlInP/GaAs substrate coated with tapered nanowires. In both graphs the total reflectance (black squares), specular reflectance (blue triangles), and diffuse reflectance (red circles) are displayed. c) Measured total transmittance through and d) measured absorbance in the AlInP/GaAs substrate (solid squares) and the AlInP/GaAs substrate coated with tapered nanowires (open squares). The solid curves correspond to the calculated reflectance, transmittance, and absorbance of the reference sample, and the dashed curves to the calculations of the nanowire sample. The inset in d) shows a photograph of the AlInP/GaAs substrate coated with nanowires and without nanowires.

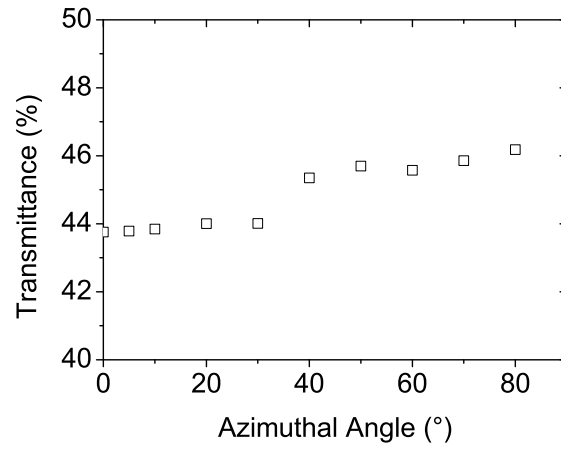


Figure 4: Measured transmittance through the AlInP/GaAs substrate coated with tapered nanowires as a function of azimuthal angle at a wavelength of 1100 nm.

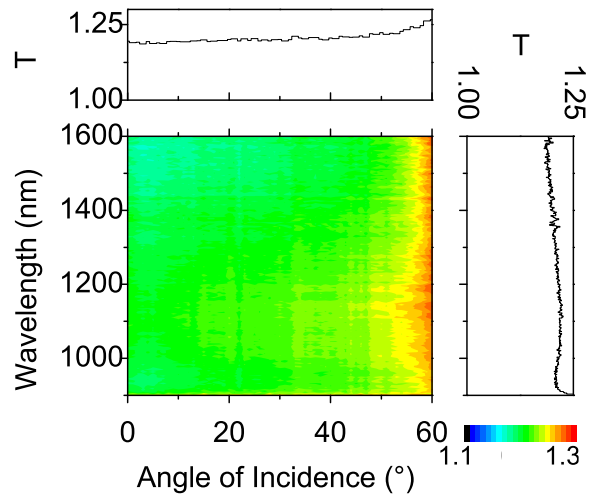


Figure 5: Measured transmission through the AlInP/GaAs substrate coated with nanowires normalized to the transmission through an AlInP/GaAs substrate as a function of angle of incidence and wavelength. The top inset shows a cut to the measurement at 1400 nm and the right inset shows a cut at an angle of incidence of 30°.

References

- [1] R. R. King, D. C. Law, K. M. Edmondson, C. M. Fetzer, G. S. Kinsey, H. Yoon, R. A. Sherif, N. H. Karam, 40% efficient metamorphic GaInP/GaInAs/Ge multijunction solar cells, *Appl. Phys. Lett.* 90 (2007) 183516.
- [2] W. Guter, J. Schne, S. P. Philipps, M. Steiner, G. Siefer, A. Wekkeli, E. Welsler, E. Oliva, A. W. Bett, F. Dimroth, Current-matched triple-junction solar cell reaching 41.1 % conversion efficiency under concentrated sunlight, *Appl. Phys. Lett.* 94 (2009) 223504.
- [3] M. Stan, D. Aiken, B. Cho, A. Cornfeld, V. Ley, P. Patel, P. Sharps, T. Varghese, High-efficiency quadruple junction solar cells using OMVPE with inverted metamorphic device structures, *Journal of Crystal Growth* 312 (2010) 1370 – 1374.
- [4] R. R. King, D. C. Law, K. M. Edmondson, C. M. Fetzer, G. S. Kinsey, H. Yoon, D. D. Krut, J. H. Ermer, R. A. Sherif, N. H. Karam, Advances in high-efficiency III-V multijunction solar cells, *Advances in OptoElectronics 2007* (2007) 29523.
- [5] D. Friedman, Progress and challenges for next-generation high-efficiency multijunction solar cells, *Current Opinion in Solid State and Materials Science* 14 (2010) 131 – 138.
- [6] D. S. Hobbs, B. D. MacLeod, J. R. Riccobono, Update on the development of high performance anti-reflecting surface relief micro-structures, *Proc. of SPIE* 6545 (2007) 65450Y.

- [7] C. G. Bernhard, Structural and functional adaption in a visual system, *Endeavour* 26 (1967) 79.
- [8] J.-Q. Xi, M. F. Schubert, J. K. Kim, E. F. Schubert, M. Chen, S.-Y. Lin, W. Liu, J. A. Smart, Optical thin-film materials with low refractive index for broadband elimination of fresnel reflection, *Nat. Photonics* 1 (2007) 176–179.
- [9] Y.-F. Huang, S. Chattopadhyay, Y.-J. Jen, C.-Y. Peng, T.-A. Liu, Y.-K. Hsu, C.-L. Pang, H.-C. Lo, C.-H. Hsu, Y.-H. Chang, C.-S. Lee, K.-H. Chen, L.-C. Chen, Improved broadband and quasi-omnidirectional anti-reflection properties with biomimetic silicon nanostructures, *Nat. Nanotech.* 2 (2007) 770–774.
- [10] Y.-J. Lee, D. S. Ruby, D. W. Peters, B. B. McKenzie, J. W. P. Hsu, ZnO nanostructures as efficient antireflection layers in solar cells, *Nano Lett.* 8 (2008) 1501.
- [11] S. L. Diedenhofen, G. Vecchi, R. E. Algra, A. Hartsuiker, O. L. Muskens, G. Immink, E. P. A. M. Bakkers, W. L. Vos, J. Gmez Rivas, Broadband and omnidirectional antireflection coatings based on semiconductor nanorods, *Adv. Mat.* 21 (2009) 973–978.
- [12] J. Tommila, V. Polojärvi, A. Aho, A. Tukiainen, J. Viheriälä, J. Salmi, A. Schramm, J. M. Kontio, A. Turtiainen, T. Niemi, M. Guina, Nanostructured broadband antireflection coatings on AlInP fabricated by nanoimprint lithography, *Solar Energy Materials and Solar Cells* 94 (2010) 1845–1848.

- [13] J. Leem, J. Yu, Y. Song, Y. Lee, Antireflective characteristics of disordered GaAs subwavelength structures by thermally dewetted Au nanoparticles, *Solar Energy Materials and Solar Cells* 95 (2011) 669 – 676.
- [14] D. Kumar, S. K. Srivastava, P. Singh, M. Husain, V. Kumar, Fabrication of silicon nanowire arrays based solar cell with improved performance, *Solar Energy Materials and Solar Cells* 95 (2011) 215 – 218.
- [15] P.-C. Tseng, P. Yu, H.-C. Chen, Y.-L. Tsai, H.-W. Han, M.-A. Tsai, C.-H. Chang, H.-C. Kuo, Angle-resolved characteristics of silicon photovoltaics with passivated conical-frustum nanostructures, *Solar Energy Materials and Solar Cells* 95 (9) (2011) 2610 – 2615.
- [16] S.-H. Baek, S.-B. Kim, J.-K. Shin, J. H. Kim, Preparation of hybrid silicon wire and planar solar cells having ZnO antireflection coating by all-solution processes, *Solar Energy Materials and Solar Cells* 96 (2012) 251 – 256.
- [17] P. Yeh, *Optical waves in layered media*, John Wiley and Sons, New York, Chichester, Brisbane, Toronto, Singapore, 1988.
- [18] E. J. Haverkamp, P. Mulder, G. J. Bauhuis, J. J. Schermer, M. M. A. J. Voncken, J. van Deelen, A. T. J. van Niftrik, P. K. Larsen, Spectrum and bandgap optimized antireflection coating by numerical simulations, in: *20th European Photovoltaic Solar Energy Conference*, 2005.
- [19] R. S. Wagner, W. C. Ellis, Vapor-liquid-solid mechanism of single crystal growth, *Appl. Phys. Lett.* 4 (1964) 89–90.

- [20] O. L. Muskens, S. L. Diedenhofen, M. H. M. van Weert, M. T. Borgström, E. P. A. M. Bakkers, J. Gómez Rivas, Epitaxial growth of aligned semiconductor nanowire metamaterials for photonic applications, *Adv. Func. Mat.* 18 (2008) 1039.
- [21] K. R. Catchpole, A. Polman, Plasmonic solar cells, *Opt. Express* 16 (26) (2008) 21793–21800.